Earth and Planetary Science Letters 403 (2014) 317–327

Contents lists available at ScienceDirect

Earth and Planetary Science Letters

www.elsevier.com/locate/epsl

Nucleosynthetic W isotope anomalies and the Hf–W chronometry of Ca–Al-rich inclusions

Thomas S. Kruijer [a,b,*], Thorsten Kleine [a], Mario Fischer-Gödde [a], Christoph Burkhardt [c], Rainer Wieler [b]

[a] Institut für Planetologie, Westfälische Wilhelms-Universität Münster, Wilhelm Klemm-Strasse 10, 48149 Münster, Germany
[b] ETH Zürich, Institute of Geochemistry and Petrology, Clausiusstrasse 25, 8092 Zürich, Switzerland
[c] Origins Laboratory, Department of the Geophysical Sciences, The University of Chicago, 5734 South Ellis Avenue, Chicago, IL 60637, USA

ARTICLE INFO

Article history:
Received 12 September 2013
Received in revised form 1 July 2014
Accepted 4 July 2014
Available online 29 July 2014
Editor: T. Elliott

Keywords:
Hf–W chronometry
CAI
^{26}Al
early solar system
chronology
nucleosynthetic isotope anomalies

ABSTRACT

Ca–Al-rich inclusions (CAI) are the oldest dated objects formed in the solar system and are pivotal reference points in early solar system chronology. Knowledge of their initial ^{182}Hf/^{180}Hf and ^{182}W/^{184}W is essential, not only for obtaining precise Hf–W ages relative to the start of the solar system, but also to assess the distribution of short-lived radionuclides in the early solar nebula. However, the interpretation of Hf–W data for CAI is complicated by nucleosynthetic W isotope variations. To explore their extent and nature, and to better quantify the initial Hf and W isotope compositions of the solar system, we obtained Hf–W data for several fine- and coarse-grained CAI from three CV3 chondrites. The fine-grained CAI exhibit large and variable anomalies in ε^{183}W (ε^{i}W equals 0.01% deviation from terrestrial values), extending to much larger anomalies than previously observed in CAI, and reflecting variable abundances of *s*- and *r*-process W isotopes. Conversely, the coarse-grained (mostly type B) inclusions show only small (if any) nucleosynthetic W isotope anomalies. The investigated CAI define a precise correlation between initial ε^{182}W and ε^{183}W, providing a direct empirical means to correct the ε^{182}W of any CAI for nucleosynthetic isotope anomalies using their measured ε^{183}W. After correction for nucleosynthetic W isotope variations, the CAI data define an initial ^{182}Hf/^{180}Hf of $(1.018 \pm 0.043) \times 10^{-4}$ and an initial ε^{182}W of -3.49 ± 0.07. The Hf–W formation intervals of the angrites D'Orbigny and Sahara 99555 relative to this CAI initial is 4.8 ± 0.6 Ma, in good agreement with Al–Mg ages of these two angrites. This renders a grossly heterogeneous distribution of ^{26}Al in the inner solar system unlikely, at least in the region were CAI and angrites formed.

1. Introduction

The timespan between condensation of the first solids and melting and differentiation of the first planetary bodies probably was only a few million years (Ma). Distinguishing between different events and establishing a fine-scale chronology of early solar system evolution, therefore, requires the determination of highly precise ages for meteorites and meteorite components. The necessary time resolution is in principle provided by Pb–Pb chronometry (*e.g.*, Amelin et al., 2002, 2010; Bouvier and Wadhwa, 2010; Connelly et al., 2012) and by several short-lived chronometers such as the ^{26}Al–^{26}Mg (*e.g.*, Jacobsen et al., 2008; Lee et al., 1976, 1977; MacPherson et al., 1995) and ^{182}Hf–^{182}W systems (*e.g.*, Kleine et al., 2009). However, the precise chronological interpretation of the isotopic data is not always straightforward, and can be hampered by (i) mass-independent isotope variations in the elements of interest (*e.g.*, Brennecka et al., 2010; Burkhardt et al., 2012; Leya et al., 2009; Wasserburg et al., 2012) and (ii) a possible heterogeneous distribution of some short-lived radionuclides (especially ^{26}Al) (*e.g.*, Clayton et al., 1977; Gounelle and Russell, 2005; Gounelle et al., 2001; Larsen et al., 2011; Lee, 1978).

The short-lived ^{182}Hf–^{182}W system ($t_{1/2} = 8.9$ Ma) is a powerful chronometer to determine the timescales of planetary differentiation and can also provide precise ages for individual meteorites (Kleine et al., 2009). Obtaining accurate and precise ^{182}Hf–^{182}W ages requires knowledge of the initial ^{182}Hf/^{180}Hf and ^{182}W/^{184}W ratios at the start of solar system history. These values can most directly be determined on Ca–Al-rich inclusions (CAI), which are the oldest objects formed in the solar system (*e.g.*, Amelin et al., 2002; Gray et al., 1973; Lee et al., 1976; Podosek et al., 1991), and are

* Corresponding author at: Institut für Planetologie, Westfälische Wilhelms-Universität Münster, Wilhelm Klemm-Strasse 10, 48149 Münster, Germany. Tel.: +49 251 83 39081.
E-mail address: thomas.kruijer@uni-muenster.de (T.S. Kruijer).

http://dx.doi.org/10.1016/j.epsl.2014.07.003
0012-821X/

commonly used to define 'time-zero' in early solar system chronology as recorded in meteorites. So far mostly coarse-grained CAI have been investigated for Hf–W isotope systematics (Burkhardt et al., 2008), but the interpretation of these data is complicated by the presence of nucleosynthetic W isotope anomalies in the CAI (Burkhardt et al., 2012). High precision measurements of both $^{182}W/^{184}W$ and $^{183}W/^{184}W$ on bulk CAI, and knowledge of the relative nucleosynthetic contributions to ^{182}W and ^{183}W anomalies are, therefore, required to quantify the extent and nature of nucleosynthetic W isotope anomalies in CAI, which in turn is essential to tightly constrain the initial $^{182}Hf/^{180}Hf$ and $^{182}W/^{184}W$ of the solar system.

Fine-grained CAI have so far not been systematically investigated for Hf–W systematics, but several features make them particularly suited to determine the initial $^{182}Hf/^{180}Hf$ and $^{182}W/^{184}W$ of the solar system. First, most fine-grained CAI are characterized by Group II REE patterns, which are indicative of high-temperature fractional condensation of a gas of solar composition (Boynton, 1975; Davis and Grossman, 1979). This suggests that their Hf/W ratios may be different from those of coarse-grained CAI, which are characterized by mostly flat REE patterns and typically have near-chondritic Hf/W ratios. Thus, based on fine-grained CAI it may be possible to determine a bulk CAI Hf–W isochron. Second, coarse-grained CAI appear to have more variable Al–Mg ages than fine-grained CAI, suggesting that processing of coarse-grained CAI extended for ~0.2 Ma (perhaps even ~0.7 Ma) after primary CAI formation (MacPherson et al., 2012). Although such brief time intervals cannot be resolved using Hf–W chronometry, the Al–Mg data suggest that fine-grained CAI may represent the earliest-formed, least processed, and as such, most insightful objects for investigating the pristine isotopic signatures at the start of solar system history. Finally, fine-grained CAI, at least for some elements—such as Ti (*e.g.*, Niemeyer and Lugmair, 1981)—appear to show more variable and larger nucleosynthetic isotope anomalies than most coarse-grained CAI. This makes fine-grained CAI ideally suited for investigating the effects of nucleosynthetic W isotope anomalies on Hf–W chronometry.

We report new Hf–W isotope data for five fine-grained and seven coarse-grained CAI from the Allende, NWA 6870 and NWA 6717 CV3 chondrites. In addition, five separate digestion aliquots of a powdered slab (100 g) of Allende were also analyzed for their Hf–W isotope systematics. The new Hf–W data are used to assess the relative contributions to W isotope variations in CAI of (i) ^{182}Hf decay and (ii) *s*- and *r*-process variations, with the ultimate aim to more precisely constrain the initial Hf and W isotope compositions of the solar system. Based on the new Hf–W data the extent of possible heterogeneities in the initial abundance of the short-lived radionuclides ^{182}Hf and ^{26}Al in the early solar system is assessed.

2. Samples and analytical methods

2.1. Sample preparation and chemical separation

The petrographic and chemical classification (Fig. S8; Section S1) demonstrates that our CAI sample suite can be distinguished into (i) *fine-grained* CAI with Group II REE patterns and (ii) *coarse-grained* (mostly type B) CAI with mostly Group I patterns. The CAI samples (~50–300 mg) were carefully cut out of the meteorite slices using a diamond saw and then cleaned with ethanol or acetone in an ultrasonic bath to remove any adhering dust. The samples were gently crushed in an agate mortar and the cleanest CAI pieces were handpicked under a binocular microscope. Care was taken to remove any chondrite matrix material adhering to the CAI pieces. Finally, the CAI fractions were cleaned again in ethanol, dried, and ground to a fine powder.

The CAI samples were digested in 15 or 60 ml Savillex® vials in $HF–HNO_3–HClO_4$ (2 : 1 : 0.05) at 180–200 °C for 4–5 days on a hotplate. After digestion, samples were evaporated to dryness at 200 °C to remove $HClO_4$ and fluoride precipitates, and then treated by repeated dry-downs in 6 M HCl–0.06 M HF. Finally, the samples were completely dissolved in 12 ml (15 ml vials) or 40 ml (60 ml vials) 6 M HCl–0.06 M HF. Approximately 1–10% aliquots (equivalent to ~2–4 ng W) of these solutions were spiked with a mixed $^{180}Hf–^{183}W$ tracer that was calibrated against pure Hf and W metal standards (Kleine et al., 2004). Additional aliquots (2–3%) were taken to determine REE concentrations (Section S1.2.1).

Tungsten was separated from the sample matrix using a two-stage anion exchange chromatography, slightly modified from previously published procedures (Kleine et al., 2004, 2012). The aliquots for W isotope composition analyses were evaporated to dryness and re-dissolved in 13 ml 0.5 M HCl–0.5 M HF prior to loading onto the first anion exchange column (4 ml BioRad® AG 1 × 8, 200–400 mesh). The sample matrix was rinsed off the column in 10 ml 0.5 M HCl–0.5 M HF, followed by another rinse with 6 ml 6 M HCl–1 M HF in which significant amounts of Ti, Zr and Hf were eluted. Finally, W was eluted in 8 ml 6 M HCl–1 M HF. The second anion exchange chromatography step, modified after Kleine et al. (2012), provides quantitative removal of the HFSE (Ti, Zr, Hf, Ta) from the W cuts. The samples were evaporated at 200 °C with added $HClO_4$ to destroy organic molecules, re-dissolved in 0.6 M HF–0.2% H_2O_2 and loaded onto pre-cleaned BioRad® Polyprep columns filled with 1 ml anion exchange resin (AG1 × 8, 200–400). Titanium, Zr, and Hf were rinsed off the column with 10 ml 1 M HCl–2% H_2O_2, followed by 10 ml 8 M HCl–0.01 M HF. Finally, W was eluted in 8 ml 6 M HCl–1 M HF. The W cuts were evaporated to dryness with added $HClO_4$ (200 °C) and converted to 0.56 M HNO_3–0.24 M HF measurement solutions. The chemical separation of Hf and W for the spiked aliquots was accomplished using ion exchange chromatography techniques described in Kleine et al. (2004).

Total procedural blanks ranged from ~70 to ~120 pg for the W isotope composition analyses, and ~5 to ~30 pg W and ~2 to ~5 pg Hf for the isotope dilution analyses. The corresponding blank corrections for W isotope composition measurements were <4 ppm on $\varepsilon^{182}W$, and hence, negligible given the analytical resolution of our data. The blank corrections for the isotope dilution analyses were mostly $\lesssim$3% for both Hf and W, and were included in the uncertainty of the $^{180}Hf/^{184}W$ assuming an average uncertainty on the blank correction of 50% (Table 1). In a few cases, the blank corrections were slightly larger (up to 6%), primarily due to the low Hf and W amounts available for analysis.

2.2. Isotope measurements

All isotope measurements were performed with a ThermoScientific® Neptune *Plus* MC-ICPMS in the Institut für Planetologie at the University of Münster. Tungsten was introduced into the mass spectrometer using an ESI® PFA nebulizer connected to a Cetac® Aridus II desolvator. A combination of high-sensitivity Jet sampler and X skimmer cones was used and total ion beam intensities of $2–2.5 \times 10^{-10}$ A were obtained for a 30 ppb W solution at a 50–60 µL/min uptake rate. Each measurement consisted of 60 s baseline integrations (deflected beam) followed by 200 isotope ratio measurements of 4.2 s each. Possible isobaric interferences of Os on ^{184}W and ^{186}W were corrected by monitoring interference-free ^{188}Os and were negligible (<10 ppm on $\varepsilon^{182}W$) for all analyzed samples. Instrumental mass bias was corrected by internal normalization to either $^{186}W/^{183}W = 1.9859$ (denoted '6/3') or $^{186}W/^{184}W = 0.92767$ (denoted '6/4') using the exponential law. The W isotope measurements of the analyzed samples were bracketed by measurements of a terrestrial solution standard (prepared

from an Alfa Aesar® metal, batch no. 22312; Kleine et al., 2004; 2002) and are reported as ε-unit deviations (*i.e.*, 0.01%) relative to the mean values of the bracketing standard analyses. For samples analyzed more than once, the reported ε^{i}W represent the mean of pooled solution replicates. The accuracy and reproducibility of the measurements were assessed by repeated analyses of terrestrial rock standards (BCR-2, BHVO-2) that were digested, processed through the full chemical separation, and analyzed together with each set of samples. Note that BCR-2 was processed together with the CAI samples, while BHVO-2 was processed together with the Allende bulk rock samples (Table S1).

The mean ε^{182}W (6/4) of 0.00 ± 0.16 (2 s.d., $n = 13$) obtained for the BCR-2 standard is identical to the terrestrial W isotope composition, as is the mean ε^{182}W (6/4) of -0.04 ± 0.11 (2 s.d., $n = 8$) measured for BHVO-2 (Table S1). The BCR-2 analyses show small anomalies for normalizations involving ^{183}W, however, resulting in coupled ε^{182}W (6/3)–ε^{184}W (6/3) shifts (see Section S2). These shifts have previously been observed in high-precision MC-ICPMS studies for terrestrial samples and iron meteorites and are attributed to a small odd–even isotope fractionation during sample preparation (Kruijer et al., 2013, 2012; Shirai and Humayun, 2011; Willbold et al., 2011). Accordingly, the measured ε^{182}W (6/3), ε^{183}W (6/4), and ε^{184}W (6/3) of the CAI from this study were corrected using the mean ε^{i}W values obtained for the BCR-2 samples processed together with the CAI (Table 1). No correction was required for the W isotope ratios measured for Allende in the present study, because the BHVO-2 analyses performed together with the Allende measurements did not show any resolvable mass-independent effect.

The uncertainties of the W isotope measurements were estimated based on the 2 s.d. of replicate measurements of the BCR-2 standard (if $N < 4$) or 95% conf. intervals based on multiple solution replicates (if $N \geq 4$) (see above and Table S1). The uncertainty of the Hf and W isotope dilution measurements (2σ) derives from the uncertainty on the isotope ratio measurement (0.2%, 2 s.d.) and from the blank correction (generally <3%). The resulting uncertainty on ^{180}Hf/^{184}W ratios is <1.5% (2σ) in most cases.

3. Results

The ^{180}Hf/^{184}W ratios and measured W isotope compositions of the investigated CAI are presented in Table 1 and Fig. 1. Since the magnitude of potential nucleosynthetic W isotope anomalies depend on the normalization ratio used to correct for instrumental mass fractionation (Burkhardt et al., 2012), the ε^{i}W values are shown for two different normalizations and are denoted '6/4' for normalization to ^{186}W/^{184}W and '6/3' for normalization to ^{186}W/^{183}W. The investigated CAI exhibit variable ε^{182}W (6/4) ranging from −2.5 to +4.5, while the ε^{182}W (6/3) values of the same samples show a smaller range and vary between −3.1 and +1.1 (Table 1). The fine-grained CAI exhibit variable ε^{183}W (6/4) with excesses of up to +5.3, whereas the ε^{183}W of most coarse-grained CAI are indistinguishable from the terrestrial W isotope composition. Samples with elevated ε^{183}W also display marked differences between ε^{182}W (6/4) and ε^{182}W (6/3) which scale with the magnitude of the ^{183}W anomaly.

The ^{180}Hf/^{184}W ratios of the fine-grained CAI are variable and range from ∼0.3 to ∼3.3, whereas the coarse-grained CAI investigated here and in previous studies (Burkhardt et al., 2008; Kleine et al., 2005) exhibit less variable ^{180}Hf/^{184}W ratios, which are in the range of those of chondrites. For type B CAI AI01 a substantially higher ^{180}Hf/^{184}W of ∼3.9 was determined, but this CAI is exceptionally large and it is unclear whether the analyzed piece is representative for the bulk CAI. The ε^{182}W (6/3) values of the CAI are linearly correlated with their ^{180}Hf/^{184}W, but no such correlation is observed for the ε^{182}W (6/4) values (Fig. 1c, d). This reflects that the ε^{182}W values obtained in the two different normalizations are distinct for some of the investigated CAI.

The five replicates of a bulk Allende powder yield a mean ε^{182}W (6/4) of -1.97 ± 0.04 (95% conf., $n = 5$), and a mean ^{180}Hf/^{184}W of 1.35 ± 0.03 (95% conf., $n = 5$) (Table S2). The mean ε^{183}W of 0.02 ± 0.05 obtained here for Allende is indistinguishable from the terrestrial value and from the mean obtained for replicate measurements of the BHVO-2 samples processed together with Allende (Table S1).

4. Nucleosynthetic W isotope anomalies in CAI

Variations in ε^{182}W may be (i) radiogenic (*i.e.*, from ^{182}Hf-decay), (ii) nucleosynthetic (*e.g.*, reflecting a heterogeneous distribution of *s*- and *r*-process W nuclides), or (iii) cosmogenic (*i.e.*, resulting from the interaction with secondary neutrons produced by interaction with cosmic rays). Model calculations for neutron capture effects on W isotopes in carbonaceous chondrites reveal that the neutron capture reaction ^{181}Ta(n, γ)^{182}Ta and subsequent β^{-}-decay to ^{182}W can be relevant for CAI minerals having high Ta/W ratios (Leya, 2011). However, this effect will likely be small in bulk CAI, which generally have low Ta/W. Although the Ta/W ratios of the CAI have not been determined directly in the present study, they can be inferred assuming that the CAI have chondritic Ta/Hf (Lodders, 2003). This results in inferred Ta/W of ∼0.03–0.4 for the investigated CAI. The model from Leya (2011) predicts that for this range in Ta/W and for a relatively short exposure age of ∼5.2 Ma for Allende (Scherer and Schultz, 2000), any neutron capture effects in the investigated CAI will be <0.05 ε^{182}W units. Given the analytical resolution of the W isotope data, cosmic-ray effects can thus be considered negligible.

Variations in ε^{183}W can only be nucleosynthetic in origin and as such can be used to assess the extent of nucleosynthetic W isotope variations in a given sample (note that there are no resolvable cosmogenic effects on ε^{183}W, because after mass bias correction the upward shift of ^{183}W/^{184}W is compensated by downward shifts in the normalization ratios ^{186}W/^{183}W and ^{186}W/^{184}W; Leya et al., 2003; Kleine et al., 2005). Since ^{184}W has a larger relative *s*-process contribution than ^{182}W, ^{183}W and ^{186}W, a deficit in *s*-process (or an excess in *r*-process) W nuclides results in elevated ε^{183}W. The elevated ε^{183}W of most of the investigated *fine-grained* CAI, therefore, indicates an *s*-deficit (or *r*-excess) in these samples. One fine-grained CAI (AF04) shows a very large anomaly in ε^{183}W (∼+5.3), about two times the largest anomaly so far observed for CAI, namely CAI A-ZH-5 (Burkhardt et al., 2008; 2012). In contrast, all of the *coarse-grained* (mostly type B) inclusions investigated here show near-terrestrial ε^{183}W, indicating that nucleosynthetic W isotope heterogeneity is largely absent in these samples. Conversely, the three type B CAI investigated by Burkhardt et al. (2008, 2012) have elevated measured ε^{183}W. Note that any potential analytical artefact on ^{183}W in these CAI akin to that observed in the present study (see above and Section S2.1.1) would make their measured ε^{183}W anomalies seem smaller, so the measured values should be considered minimum estimates. Thus, both coarse- and fine-grained CAI exhibit nucleosynthetic W isotope heterogeneities, but the ε^{183}W anomalies of type B CAI in general seem smaller and more uniform in comparison with the large and variable nucleosynthetic W isotope anomalies of fine-grained CAI (Table 1).

The extent of nucleosynthetic ^{182}W variability is more difficult to assess, because the ε^{182}W values of the CAI result from a combination of nucleosynthetic and radiogenic effects. This is illustrated in a plot of ε^{182}W *vs.* ε^{183}W, in which the data strongly scatter and do not plot along the trend expected for correlated nucleosynthetic ^{182}W and ^{183}W anomalies (Fig. 1a). Determining the magnitude of nucleosynthetic ^{182}W anomalies, therefore, first re-

Table 1
Hf–W data for bulk CAI.

ID	Meteorite	Type	REE pattern	Weight (mg)	Hf (ng/g)	W (ng/g)	$^{180}Hf/^{184}W$ ($\pm 2\sigma$)	N	$\varepsilon^{182/184}W_{meas.}$ ($\pm$2 s.d.)	$\varepsilon^{183/184}W_{meas.}$ ($\pm$2 s.d.)[a]	$\varepsilon^{182}W_i$ ($\pm$2 s.d.)[b]	$\varepsilon^{182}W_{nuc.\ corr.}$ ($\pm$2 s.d.)[c]	$\varepsilon^{182/183}W_{meas.}$ ($\pm$2 s.d.)[a]	$\varepsilon^{184/183}W_{meas.}$ ($\pm$2 s.d.)[a]	$\varepsilon^{182}W_i$ ($\pm$2 s.d.)[b]	$\varepsilon^{182}W_{nuc.\ corr.}$ ($\pm$2 s.d.)[c]
									Normalization to $^{186}W/^{184}W$				Normalization to $^{186}W/^{183}W$			
Fine-grained CAI																
AC01	Allende	FG	n.d.	52	1087	477[d]	2.689 ± 0.096	1	−0.33 ± 0.16	−0.01 ± 0.19	−3.48 ± 0.31	−0.32 ± 0.30	−0.29 ± 0.17	0.01 ± 0.12	−3.45 ± 0.24	−0.29 ± 0.17
AF01	Allende	FG	Group II	289	252	89.8	3.311 ± 0.029	1	3.35 ± 0.16	2.04 ± 0.19	−0.54 ± 0.33	0.47 ± 0.33	0.56 ± 0.17	−1.36 ± 0.12	−3.33 ± 0.24	0.41 ± 0.18
AF02	Allende	FG	Group II	120	33.0[d]	97.0	0.402 ± 0.005	1	−1.01 ± 0.16	1.53 ± 0.22	−1.48 ± 0.16	−3.16 ± 0.36	−3.02 ± 0.19	−1.02 ± 0.15	−3.49 ± 0.19	−3.13 ± 0.20
AF03	Allende	FG	Group II	34	51.8[d]	108	0.564 ± 0.008	1	−2.33 ± 0.40	0.57 ± 0.37	−2.99 ± 0.40	−3.12 ± 0.66	−3.05 ± 0.34	−0.38 ± 0.25	−3.71 ± 0.34	−3.09 ± 0.34
AF04	Allende	FG	Group II	288	63.8	241	0.313 ± 0.002	2	4.47 ± 0.16	5.36 ± 0.19	4.10 ± 0.16	−3.07 ± 0.44	−2.68 ± 0.17	−3.56 ± 0.12	−3.04 ± 0.17	−3.08 ± 0.25
A-ZH-5[e]	Allende	FG+A	Group III	90	2046	1342	1.79 ± 0.01	3	2.21 ± 0.20	2.57 ± 0.36	0.11 ± 0.25	−1.41 ± 0.57	−1.14 ± 0.39	−1.71 ± 0.24	−3.25 ± 0.40	−1.33 ± 0.40
Coarse-grained CAI																
AC02	Allende	n.d.	n.d.	104	193	158[d]	1.442 ± 0.048	1	−1.58 ± 0.24	0.00 ± 0.19	−3.27 ± 0.28	−1.58 ± 0.35	−1.55 ± 0.26	0.00 ± 0.12	−3.25 ± 0.28	−1.55 ± 0.26
AF05	Allende	B	Group I	69	1725	1224	1.662 ± 0.009	2	−1.19 ± 0.16	0.07 ± 0.19	−3.12 ± 0.21	−1.28 ± 0.30	−1.26 ± 0.17	−0.04 ± 0.12	−3.20 ± 0.21	−1.26 ± 0.17
AI01	NWA 6870	B	Group I	82	2823	847	3.935 ± 0.030	2	0.95 ± 0.16	−0.09 ± 0.19	−3.67 ± 0.38	1.08 ± 0.30	1.11 ± 0.17	0.06 ± 0.12	−3.53 ± 0.26	1.11 ± 0.17
AI02	NWA 6717	B	Group II	103	311	370	0.991 ± 0.013	1	−2.52 ± 0.16	−0.17 ± 0.19	−3.68 ± 0.18	−2.29 ± 0.30	−2.29 ± 0.17	0.11 ± 0.12	−3.46 ± 0.18	−2.28 ± 0.17
AI05	Allende	n.d.	n.d.	77	230	162	1.683 ± 0.016	1	−1.15 ± 0.20	0.02 ± 0.19	−3.11 ± 0.24	−1.18 ± 0.32	−1.15 ± 0.22	−0.02 ± 0.12	−3.11 ± 0.25	−1.15 ± 0.22
AI06B	Allende	B	Group I	168	1861	1500	1.464 ± 0.009	4	−1.71 ± 0.12	−0.01 ± 0.14	−3.43 ± 0.18	−1.70 ± 0.23	−1.72 ± 0.15	0.01 ± 0.09	−3.44 ± 0.16	−1.72 ± 0.15
AI07	Allende	A	Group I	137	1081	1098	1.162 ± 0.006	4	−2.04 ± 0.12	0.03 ± 0.14	−3.40 ± 0.16	−2.08 ± 0.23	−2.09 ± 0.15	−0.02 ± 0.09	−3.46 ± 0.16	−2.09 ± 0.15
A-ZH-1[e]	Allende	B	n.d.	120	1595	1026	1.83 ± 0.01	4	−1.23 ± 0.43	0.18 ± 0.59	−3.38 ± 0.46	−1.48 ± 0.94	−1.50 ± 0.66	−0.12 ± 0.39	−3.65 ± 0.66	−1.51 ± 0.66
A-ZH-2[e]	Allende	B	Group I	180	2087	1218	2.02 ± 0.01	6	−0.80 ± 0.21	0.29 ± 0.23	−3.17 ± 0.28	−1.21 ± 0.39	−1.20 ± 0.26	−0.19 ± 0.16	−3.58 ± 0.28	−1.22 ± 0.26
A-ZH-4[e]	Allende	B	Group I	200	1731	965	2.12 ± 0.01	2	−0.55 ± 0.62	0.54 ± 0.35	−3.04 ± 0.65	−1.31 ± 0.80	−1.25 ± 0.46	−0.36 ± 0.23	−3.75 ± 0.47	−1.29 ± 0.46

Notes: Instrumental mass fractionation was corrected using the exponential law by internal normalization to $^{186}W/^{184}W = 0.92767$ (6/4) or $^{186}W/^{183}W = 1.98594$ (6/3). The uncertainties reported for measured (subscript 'meas.') $\varepsilon^{i}W$ values represent the 2 s.d. obtained from repeated analyses of the terrestrial standard BCR-2 (Table S1) in case $N < 4$, or in case $N \geq 4$, the 95% confidence limits of the mean (*i.e.*, according to: s.d. $\times\ t_{0.95,N-1}/\sqrt{N}$). Four CAI (AC02, AF02, AF03, AI05) had larger in-run errors (2 s.e.) than the estimated 2 s.d.; for these samples internal uncertainties (2 s.e.) are reported.

[a] Corrected for a mass-independent effect on ^{183}W using the average $\varepsilon^{i}W$ obtained for the BCR-2 standard: $\varepsilon^{183}W$ (6/4) $= -0.08 \pm 0.05$, $\varepsilon^{182}W$ (6/3) $= +0.12 \pm 0.08$, $\varepsilon^{184}W$ (6/3) $= +0.05 \pm 0.03$ (95% conf., $n = 13$). The added uncertainty induced by this correction is included in the reported uncertainties of measured $\varepsilon^{i}W$ values.

[b] '$\varepsilon^{182}W_i$': $\varepsilon^{182}W_{meas.}$ corrected for radiogenic contributions from ^{182}Hf decay using measured $^{180}Hf/^{184}W$ and solar system initial $^{182}Hf/^{180}Hf$ of $(1.018 \pm 0.043) \times 10^{-4}$ for the $^{186}W/^{183}W$-normalized data and $(1.015 \pm 0.076) \times 10^{-4}$ for the $^{186}W/^{184}W$-normalized data. Uncertainties of individual $\varepsilon^{182}W_i$ values were obtained by propagating the uncertainties on all parameters involved (Section S3).

[c] '$\varepsilon^{182}W_{nuc.\ corr.}$': $\varepsilon^{182}W_{meas.}$ values corrected for nucleosynthetic W isotope heterogeneity using measured $\varepsilon^{184}W$ (or $\varepsilon^{183}W$) and the regression-derived slopes shown in Fig. 2. The uncertainties of individual $\varepsilon^{182}W_{nuc.\ corr.}$ values were obtained by propagating the uncertainties of individual $\varepsilon^{182}W_{meas.}$ and $\varepsilon^{184}W$ (or $\varepsilon^{183}W$) values and the regression-derived $\varepsilon^{182}W$ *vs.* $\varepsilon^{184}W$ (or $\varepsilon^{182}W$ *vs.* $\varepsilon^{183}W$) slopes from Fig. 2 (Section S3).

[d] Concentrations with blank corrections >3%. The uncertainty on the blank corrections are assumed to be 50% and are propagated in the uncertainties of the $^{180}Hf/^{184}W$ ratios.

[e] Data from Burkhardt et al. (2008, 2012): The reported uncertainties on measured $\varepsilon^{182}W$, $\varepsilon^{184}W$, and $\varepsilon^{183}W$ represent 2 s.d. (see Section S2).

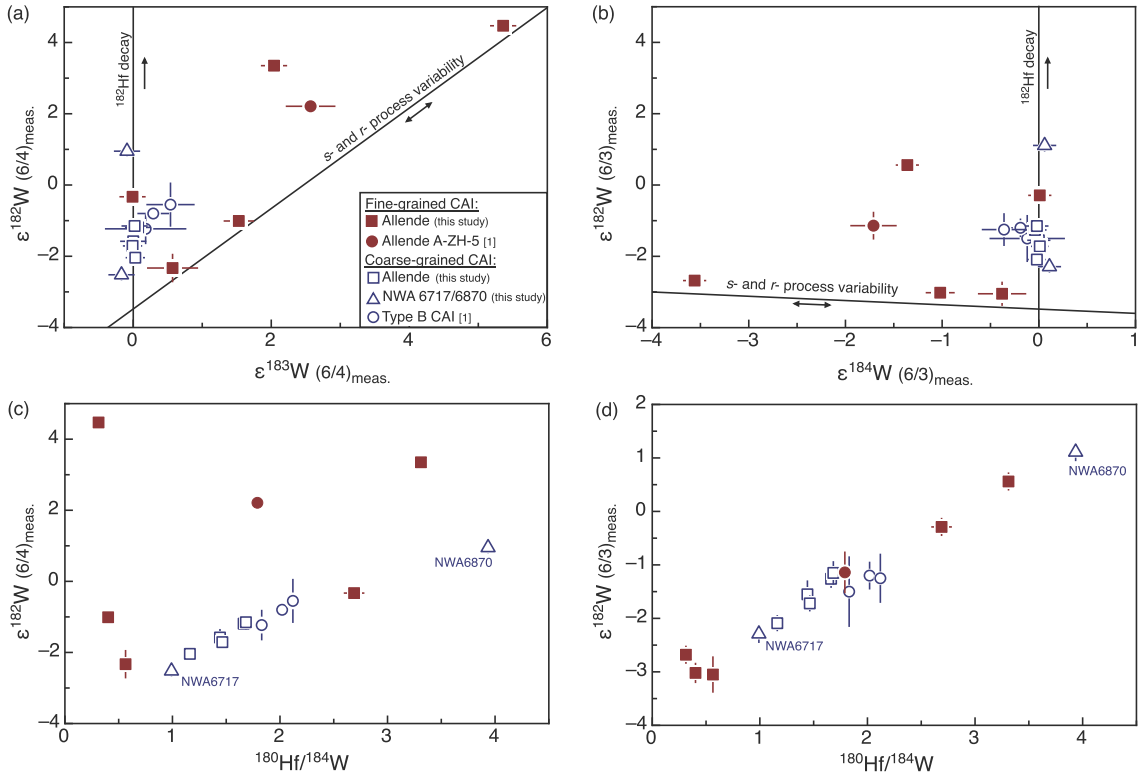

Fig. 1. Measured ε^{182}W, ε^{183}W, and ε^{184}W of CAI (a, b) and Hf–W isochron diagrams with measured ε^{182}W values (c, d). The data are shown for normalization to ^{186}W/^{184}W (a, c) and ^{186}W/^{183}W (b, d). Error bars represent external uncertainties (2 s.d.). Also plotted are the W isotope data for Allende CAI from [1] Burkhardt et al. (2008). Further shown are the effects of (i) radiogenic contributions from ^{182}Hf decay and, as a means of illustration, (ii) trends predicted for variability in *s*- and *r*-process W isotopes based on W isotope data for acid leachates from Murchison, Orgueil and Allende (Burkhardt et al., 2012; Burkhardt and Schönbächler, 2013). Note that the *s*- and *r*-process mixing line has been forced through the initial ε^{182}W of CAI.

quires the quantification of the radiogenic ingrowth in each of the CAI. This will be discussed in detail further below (Section 5).

The observed variability in nucleosynthetic W isotope anomalies in the investigated CAI raises the question of why large and variable ε^{183}W anomalies exist in fine-grained CAI, whereas coarse-grained CAI show only small if any nucleosynthetic W isotope anomalies. Since fine-grained CAI in Allende are heavily altered (*e.g.*, Grossman and Ganapathy, 1976; Kornacki and Wood, 1985; Krot et al., 1995), their nucleosynthetic W isotope anomalies could reflect the incongruent dissolution of pre-solar carrier phases and the mobilization of the released W during parent body alteration (*e.g.*, Yokoyama et al., 2011). However, significant parent body processing would also have disturbed the Hf–W systematics, but as will be shown below (Section 5), most investigated bulk CAI plot on a single Hf–W isochron whose initial ^{182}Hf/^{180}Hf, when converted to an absolute time scale, corresponds to the age of CAI as given by Pb–Pb chronometry. Hence, significant secondary disturbance of the Hf–W systematics seems unlikely (unless it occurred right at the time of CAI formation).

Alternatively, the large and variable nucleosynthetic W isotope anomalies in the fine-grained CAI reflect initial heterogeneities in the primitive solar nebula, indicating that the solar nebula was heterogeneous at the scale of individual CAI. It is noteworthy that this heterogeneity does not seem to have been sampled by the coarse-grained CAI, which generally show only small if any ^{183}W anomalies. This would suggest that fine- and coarse-grained CAI derive from two distinct nebular reservoirs, which existed at the same time but consisted of different mixtures of presolar components. Identifying the distinct nucleosynthetic components present in the precursor material of both fine- and coarse-grained CAI should be a focus of future research.

5. ^{182}Hf–^{182}W systematics of bulk CAI

The fine-grained CAI investigated in the present study display a large range in Hf/W (Table 1; Fig. 1), and are characterized by group II REE patterns, which are indicative of fractional condensation in the solar nebula (Boynton, 1975; Davis and Grossman, 1979). Their variable Hf/W ratios, therefore, probably result from chemical fractionation during condensation of the CAI, making it possible to determine a bulk CAI isochron. However, given the evidence for large and variable nucleosynthetic W isotope anomalies in the investigated CAI, the ε^{182}W values of the CAI first must be corrected for nucleosynthetic anomalies before a bulk isochron can be obtained. Below we first quantify the magnitude of nucleosynthetic W isotope heterogeneity using the ε^{182}W *vs.* ε^{183}W correlation of the CAI (Section 5.1), and then evaluate the ^{182}Hf–^{182}W systematics of bulk CAI (Section 5.2).

5.1. Effects of nucleosynthetic W isotope anomalies on Hf–W systematics

The correction of measured ε^{182}W values for nucleosynthetic W isotope anomalies requires knowledge of the relative effects of such anomalies on ε^{182}W and ε^{183}W (or ε^{184}W). This information is provided by the slope of ε^{182}W *vs.* ε^{183}W (or ε^{184}W) correlation lines and can in principle be obtained from (i) theoretical models for nucleosynthesis (Arlandini et al., 1999), (ii) W isotope data for presolar SiC grains (Ávila et al., 2012) or acid leachates from primitive chondrites (Burkhardt et al., 2012), or (iii) empirical W isotope correlations obtained from bulk CAI. As the uncertainties of theoretical models and SiC data are large or difficult to assess, using empirical W isotope data for meteorites and their components provides the most direct and precise means to correct mea-

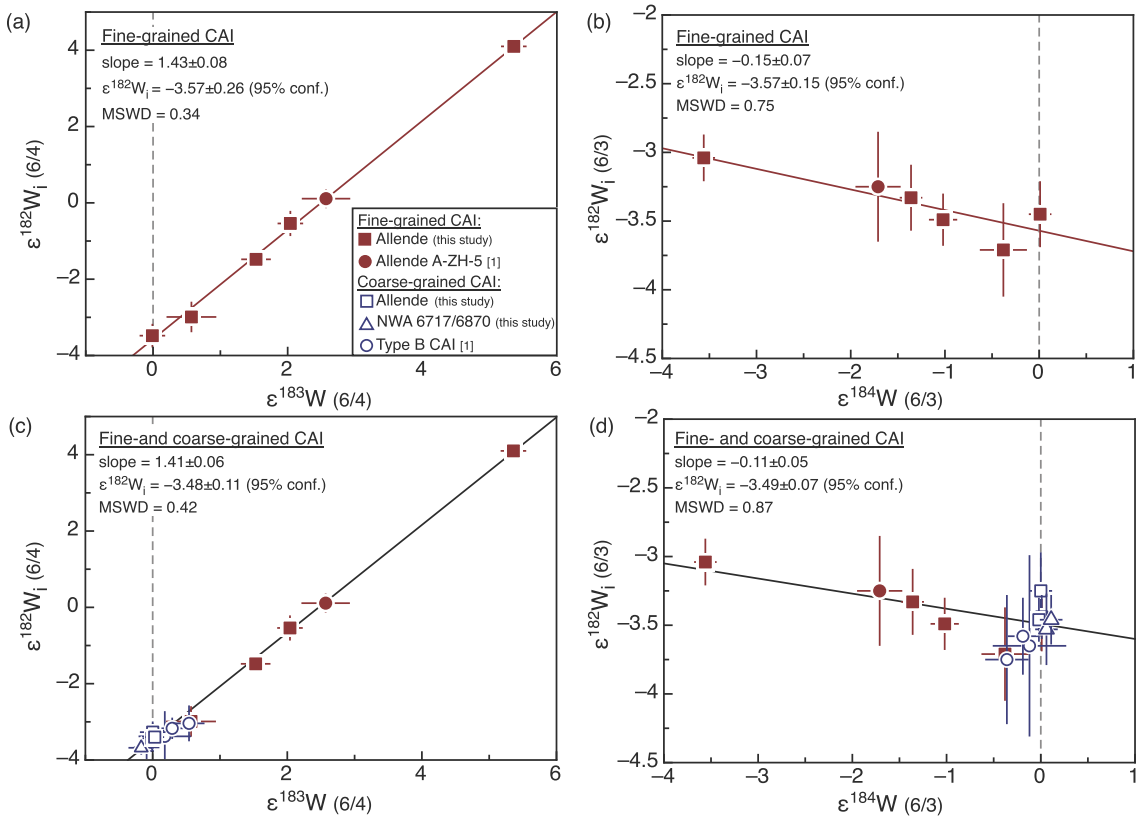

Fig. 2. Tungsten isotope systematics of bulk CAI after correction for radiogenic contributions from ^{182}Hf decay. (a, c) $\varepsilon^{182}W_i$ (6/4) *vs.* ε^{183}W (6/4) and (b, d) $\varepsilon^{182}W_i$ (6/3) *vs.* ε^{184}W (6/3). Shown are data and regressions for fine-grained CAI only (a, b), and for both fine- and coarse-grained CAI (c, d). The corrections for ^{182}Hf decay were calculated using the measured ^{180}Hf/^{184}W and a solar system initial of $^{182}Hf/^{180}Hf_{SSI} = (1.018 \pm 0.043) \times 10^{-4}$ (95% conf.) for the ^{186}W/^{183}W normalized data, and $^{182}Hf/^{180}Hf_i = (1.015 \pm 0.076) \times 10^{-4}$ for the ^{186}W/^{184}W normalized data. Error bars on symbols indicate external measurement uncertainties (2 s.d.) in case of ε^{183}W and ε^{184}W, and propagated uncertainties for decay-corrected $\varepsilon^{182}W_i$ (2 s.d.). Solid lines show linear regressions through the data calculated using Isoplot. Also shown are data for Allende CAI [1] from Burkhardt et al. (2008).

sured ε^{182}W values for nucleosynthetic W isotope variability. This is particularly true for the fine-grained CAI from this study, which exhibit large and variable nucleosynthetic isotope anomalies, and hence, permit the determination of a precise ε^{182}W–ε^{183}W (or ε^{184}W) correlation line.

Investigating the co-variation of nucleosynthetic anomalies on ε^{182}W and ε^{183}W requires correction of the ε^{182}W anomalies for radiogenic contributions from ^{182}Hf-decay. However, such corrections require knowledge about the initial ^{182}Hf/^{180}Hf of the solar system, which is the parameter that we ultimately aim to determine using a bulk CAI isochron. The slope of the correlation lines for nucleosynthetic ε^{182}W, ε^{183}W and ε^{184}W anomalies and the initial ^{182}Hf/^{180}Hf of CAI, therefore, must be determined using an iterative approach as follows: First, the initial ^{182}Hf/^{180}Hf of CAI must be estimated and here we used a value of $(9.85 \pm 0.71) \times 10^{-5}$ obtained from the linear regression of *measured* ε^{182}W (6/3) *vs.* ^{180}Hf/^{184}W obtained in the present study (Fig. 1d). For the ^{186}W/^{183}W-normalization the effects of nucleosynthetic W isotope anomalies on ε^{182}W are small, such that using the *measured* ε^{182}W (6/3) in the regression already provides a reasonable estimate of the initial ^{182}Hf/^{180}Hf of the CAI. In the second step, the measured ε^{182}W (6/3) and ε^{182}W (6/4) of the investigated CAI are corrected for ^{182}Hf-decay using their measured ^{180}Hf/^{184}W and the initial ^{182}Hf/^{180}Hf of CAI. An empirical correlation is then obtained by plotting the decay-corrected "$\varepsilon^{182}W_i$" *vs.* the measured ε^{184}W (or ε^{183}W) of all CAI. Subsequently, the measured ε^{182}W of the CAI are corrected for nucleosynthetic W isotope heterogeneity using their measured ε^{184}W (or ε^{183}W) and the regression-derived $\varepsilon^{182}W_i$ *vs.* ε^{184}W (6/3) (or $\varepsilon^{182}W_i$ *vs.* ε^{183}W (6/4)) slopes defined by the CAI. The corrected ε^{182}W values are then plotted versus their ^{180}Hf/^{184}W to obtain a bulk CAI isochron, its slope providing a new initial ^{182}Hf/^{180}Hf of the CAI. After repeating the above iteration once, the inferred initial ^{182}Hf/^{180}Hf and $\varepsilon^{182}W_i$–ε^{183}W (or ε^{184}W) slopes converge to constant values (Figs. 2, 4). After the iteration, the fine-grained CAI exhibit a well-defined empirical $\varepsilon^{182}W_i$ *vs.* ε^{183}W (6/4) correlation (Fig. 2a) with a slope of $+1.43 \pm 0.08$ and an intercept $\varepsilon^{182}W_i$ of -3.57 ± 0.26 (95% conf.; Table 2). For the $\varepsilon^{182}W_i$ *vs.* ε^{184}W (6/3) correlation line a slope of -0.15 ± 0.07 and an intercept $\varepsilon^{182}W_i = -3.57 \pm 0.15$ (95% conf.) are obtained (Fig. 2b), the latter being in good agreement with the intercept value obtained for the ^{186}W/^{184}W normalization.

The coarse-grained (mostly type B) CAI from this study and from Burkhardt et al. (2008, 2012) exhibit only small (if any) nucleosynthetic W isotope anomalies and plot close to the intercept of the $\varepsilon^{182}W_i$ *vs.* ε^{183}W and $\varepsilon^{182}W_i$ *vs.* ε^{184}W correlations (Fig. 2c, d). Regression of the combined $\varepsilon^{182}W_i$–ε^{183}W (6/4) data for both fine- and coarse-grained CAI from this study and from Burkhardt et al. (2008, 2012) yields a slope of $+1.41 \pm 0.06$ and an intercept $\varepsilon^{182}W_i$ (6/4) of -3.48 ± 0.11 (95% conf.). Regression of the $\varepsilon^{182}W_i$–ε^{184}W (6/3) correlation yields a slope of -0.11 ± 0.05 and an intercept $\varepsilon^{182}W_i$ (6/3) of -3.49 ± 0.07 (95% conf.). All these values are indistinguishable from, albeit more precise than those obtained by regressing only the data of the fine-grained CAI (Table 2). Excluding the data for type B CAI from Burkhardt et al. (2008, 2012) yields indistinguishable and comparatively precise slope and intercept values (Table 2). The empirical ε^{182}W *vs.* ε^{183}W (6/4) slope obtained here from bulk CAI data is in good agreement with the slope of $+1.42 \pm 0.06$ obtained for acid leachates from the Orgueil, Murchison and Allende carbonaceous

Table 2
Linear regression results for Hf–W data of bulk CAI.

ε^{182}W-ε^{i}W correlations		Normalization to ^{186}W/^{184}W			Normalization to ^{186}W/^{183}W		
		$\varepsilon^{182/184}$W (6/4)$_i$ (95% conf.)	ε^{182}W$_i$ vs. ε^{183}W slope (95% conf.)	MSWD	$\varepsilon^{182/183}$W (6/3)$_i$ (95% conf.)	ε^{182}W$_i$ vs. ε^{184}W slope (95% conf.)	MSWD
1	Fine-grained CAI	This study & A-ZH-5 [1]	−3.57 ± 0.26	1.43 ± 0.08	0.32	−3.57 ± 0.15	−0.15 ± 0.07	0.75
2	Fine- & coarse-grained CAI	This study (excl. AF05+AI05)	−3.46 ± 0.12	1.41 ± 0.06	0.40	−3.48 ± 0.07	−0.11 ± 0.05	0.95
3	Fine- & coarse-grained CAI	This study (inc. AF05+AI05), A-ZH-5 + type B CAI [1]	−3.41 ± 0.10	1.40 ± 0.06	0.62	−3.42 ± 0.07	−0.09 ± 0.05	1.6
4	Fine- & coarse-grained CAI	This study (inc. AF05, excl. AI05), A-ZH-5 + type B CAI [1]	−3.44 ± 0.11	1.40 ± 0.06	0.48	−3.44 ± 0.07	−0.10 ± 0.05	1.4
5	Fine- & coarse-grained CAI	This study (excl. AF05+AI05), A-ZH-5 + type B CAI [1]	−3.47 ± 0.11	1.41 ± 0.06	0.36	**−3.49 ± 0.07**	−0.11 ± 0.05	0.87
Hf–W isochrons		$\varepsilon^{182/184}$W (6/4)$_i$ (95% conf.)	^{182}Hf/^{180}Hf$_i$ ($\times 10^4$, 95% conf.)	MSWD	$\varepsilon^{182/183}$W (6/3)$_i$ (95% conf.)	^{182}Hf/^{180}Hf$_i$ ($\times 10^4$, 95% conf.)	MSWD
1	Fine-grained CAI	This study & A-ZH-5 [1]	−3.61 ± 0.29	1.063 ± 0.110	0.24	−3.58 ± 0.16	1.049 ± 0.062	0.68
2	Fine- & coarse-grained CAI	This study (excl. AF05+AI05)	−3.46 ± 0.18	1.017 ± 0.076	0.44	−3.48 ± 0.11	1.020 ± 0.043	0.98
3	Fine- & coarse-grained CAI	This study (inc. AF05+AI05), A-ZH-5 + type B CAI [1]	−3.41 ± 0.17	1.009 ± 0.075	0.71	−3.42 ± 0.16	1.012 ± 0.066	2.0
4	Fine- & coarse-grained CAI	This study (inc. AF05, excl. AI05), A-ZH-5 + type B CAI [1]	−3.44 ± 0.18	1.012 ± 0.075	0.53	−3.45 ± 0.10	1.015 ± 0.043	1.5
5	Fine- & coarse-grained CAI	This study (excl. AF05+AI05), A-ZH-5 + type B CAI [1]	−3.47 ± 0.18	1.015 ± 0.076	0.39	−3.49 ± 0.10	**1.018 ± 0.043**	0.90

Notes: Best-fit regressions were calculated using Isoplot v3.41. Uncertainties represent 95% confidence intervals as given by Isoplot. Best estimates of solar system initial values are given in bold. For the isochron regressions, an average terrestrial standard W isotope composition of ^{182}W/^{184}W$_{BSE}$ = 0.864900 was used to convert ε^{182}W to ^{182}W/^{184}W. MSWD: Mean Square Weighted Deviation. [1]: Data from Burkhardt et al. (2008, 2012).

Fig. 3. ε^{182}W (6/4) *vs.* ε^{182}W (6/3) after correction for nucleosynthetic W isotope anomalies using empirically determined slopes from the ε^{182}W$_i$ *vs.* ε^{183}W and ε^{182}W *vs.* ε^{184}W correlations shown in Fig. 2. All data points plot on the 1 : 1 line, illustrating that the correction yields identical results for both normalizations. Error bars on symbols indicate external uncertainties (2 s.d.). Also shown are data for Allende CAI [1] from Burkhardt et al. (2008).

chondrites (Burkhardt et al., 2012; Burkhardt and Schönbächler, 2013). This and the observation that the corrected ε^{182}W (6/4) and ε^{182}W (6/3) values are indistinguishable (Fig. 3), shows that our iterative approach to correct the W isotope compositions of CAI for nucleosynthetic isotope heterogeneity provides consistent results.

The empirically determined ε^{182}W$_i$ *vs.* ε^{183}W (6/4) slope of $+1.41 \pm 0.06$ is slightly shallower than the slope of $\sim$+1.686 predicted by the stellar model for *s*-process nucleosynthesis of Arlandini et al. (1999). Likewise, the ε^{182}W$_i$ *vs.* ε^{184}W (6/3) slope determined here of -0.11 ± 0.05 is different from the value of $\sim$−0.524 from Arlandini et al. (1999), but is in better agreement with a slope of $\sim$+0.04 estimated by Qin et al. (2008). Given that the uncertainty of the stellar model is large and difficult to assess, the agreement between the model and the data should still be considered acceptable. Nevertheless, correcting ε^{182}W data for nucleosynthetic anomalies using models of stellar nucleosynthesis may lead to significantly different results than those obtained using the empirical slopes derived in this work. For instance, correcting the ε^{182}W$_i$ (6/4) of the fine-grained CAI AF04 using the slope predicted by the Arlandini et al. model would result in a value of −4.94 (the corrected ε^{182}W$_i$ (6/3) would be −4.91), *i.e.*, more than 1ε lower than the initial ε^{182}W of CAI derived here. Note that in a reservoir having chondritic ^{180}Hf/^{184}W a difference of $\sim$1 ε^{182}W would correspond to a calculated age difference of $\sim$10 Ma. This underlines that the quantification of nucleosynthetic isotope anomalies using empirically determined ε^{182}W$_i$ *vs.* ε^{183}W (or ε^{184}W) slopes is of paramount importance for obtaining accurate Hf–W ages.

5.2. Hf–W isochron for bulk CAI and the initial ^{182}W/^{184}W and ^{182}Hf/^{180}Hf of the solar system

After the iterative correction of ε^{182}W values for nucleosynthetic W isotope anomalies, both fine- and coarse-grained CAI plot on a single well-defined isochron (Fig. 4). The results of the isochron regressions are summarized in Table 2, and are given for both the ^{186}W/^{184}W- and ^{186}W/^{183}W-normalized data. For both normalizations consistent results are obtained, but the precision of the ^{186}W/^{183}W-normalized data is generally better than that obtained for the ^{186}W/^{184}W-normalized data. This reflects the much smaller corrections for nucleosynthetic W isotope anomalies for the former data. Also given in Table 2 are the ε^{182}W$_i$ values obtained from the intercepts of the ε^{182}W$_i$–ε^{183}W and

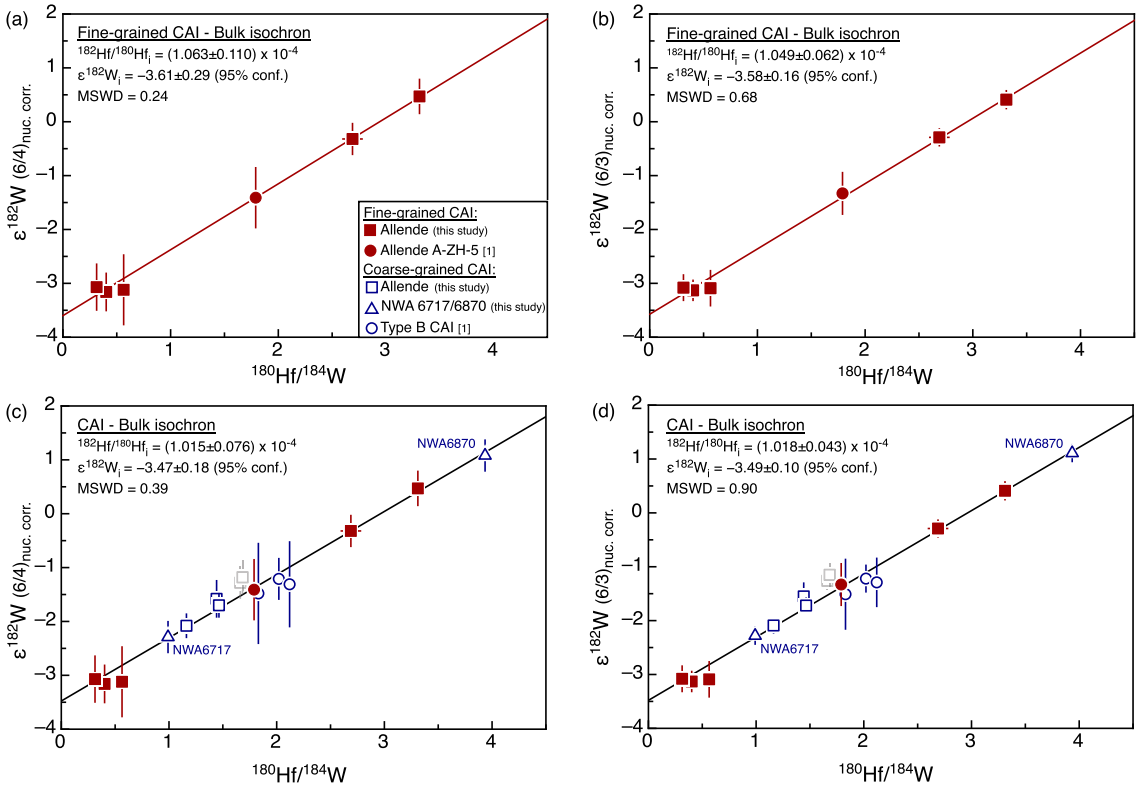

Fig. 4. Hf–W isochron diagrams for bulk CAI after iterative correction for nucleosynthetic W isotope anomalies for fine-grained CAI (a, b) and for all investigated CAI (c, d). Shown are data for normalization to $^{186}W/^{184}W$ (a, c) and $^{186}W/^{183}W$ (b, d). Error bars on symbols indicate external uncertainties and include the propagated uncertainties of the correction for nucleosynthetic W isotope anomalies (2 s.d.). The uncertainties of the corrections were calculated by propagating the individual uncertainties on all parameters involved (see Table 1 and Section S3). Solid lines show linear regressions through the data calculated using Isoplot. Note that, for reasons described in the text, Allende CAI AF05 and AI05 (grey open squares) were not included in the isochron regressions. Also shown are data for Allende CAI [1] from Burkhardt et al. (2008).

$\varepsilon^{182}W_i$–$\varepsilon^{184}W$ correlations (Fig. 2). These values are in good agreement with those obtained from the isochron regressions. Thus, two different approaches to determine the initial $\varepsilon^{182}W$ of CAI and using two different normalizations of the W isotope data provide results that are fully consistent.

A regression of all bulk CAI, including those from Burkhardt et al. (2008, 2012), gives an initial $^{182}Hf/^{180}Hf = (1.012 \pm 0.066) \times 10^{-4}$ and $\varepsilon^{182}W_i$ (6/3) $= -3.42 \pm 0.16$ (MSWD $= 2.0$). Evidence for a slight disturbance of the Hf–W systematics is provided by the near-horizontal alignment of some coarse-grained CAI in the Hf–W isochron diagram (Fig. 4), and by the observation that two coarse-grained CAI (AF05 and AI05) plot slightly above the isochron. One of them (CAI AI05) was very small and appeared strongly weathered compared to the other CAI. Excluding CAI AI05 from the regression results in an initial $^{182}Hf/^{180}Hf = (1.015 \pm 0.043) \times 10^{-4}$ and $\varepsilon^{182}W_i$ (6/3) $= -3.45 \pm 0.10$ and a slightly reduced scatter on the isochron (MSWD $= 1.5$). No independent evidence is available for secondary alteration of CAI AF05, but excluding both AI05 and AF05 from the regression results in a further reduction of the scatter (MSWD $= 0.90$) and a slightly higher initial $^{182}Hf/^{180}Hf = (1.018 \pm 0.043) \times 10^{-4}$ and lower $\varepsilon^{182}W_i$ (6/3) $= -3.49 \pm 0.10$ (Fig. 4d). This strongly suggests that the Hf–W system in both AI05 and AF05 is disturbed, and that excluding these two CAI from the isochron regression provides the best estimates for the initial $^{182}Hf/^{180}Hf$ and $\varepsilon^{182}W$ of the CAI.

Despite the evidence for slight disturbance of the Hf–W system in some CAI, several observations indicate that the overall degree of disturbance is small. First, almost all CAI plot on a single well-defined isochron, which shows no evidence for excess scatter (MSWD $= 0.90$). Second, the initial $^{182}Hf/^{180}Hf$ of $(1.018 \pm 0.043) \times 10^{-4}$ yields an absolute Hf–W age for CAI of 4567.9 ± 0.7 Ma when anchored to the angrite D'Orbigny [$^{182}Hf/^{180}Hf = (7.15 \pm 0.17) \times 10^{-5}$ (Kleine et al., 2012); Pb–Pb age $= 4563.37 \pm 0.25$ Ma (Brennecka and Wadhwa, 2012)]. This absolute Hf–W age is in very good agreement with available Pb–Pb ages of CAI, which range from ~4567 to ~4568 Ma (Amelin et al., 2010; Bouvier and Wadhwa, 2010; Connelly et al., 2012), indicating that the Hf–W isochron for bulk CAI reflects the time of Hf/W fractionation during CAI formation. Third, the preservation of large nucleosynthetic W isotope anomalies for the fine-grained CAI, and the absence of such anomalies in bulk Allende indicate that no significant diffusive W exchange with the matrix occurred during metamorphism on the CV chondrite parent body. Finally, the lack of correlation in a diagram of $\varepsilon^{182}W$ *vs.* 1/W (Fig. S10) demonstrates that the $\varepsilon^{182}W$–$^{180}Hf/^{184}W$ correlation is not a mixing line between an Hf-rich and a W-rich component, which could have potentially formed at different times (see Humayun et al., 2007). We, therefore, interpret the initial $^{182}Hf/^{180}Hf$ and $\varepsilon^{182}W$ obtained from the bulk CAI isochron as representative for the time of CAI formation, and hence, as solar system initial values. The best estimates for these values are $^{182}Hf/^{180}Hf = (1.018 \pm 0.043) \times 10^{-4}$, as obtained from the CAI isochron, and $\varepsilon^{182}W_i$ (6/3) $= -3.49 \pm 0.07$, as obtained from the $\varepsilon^{182}W_i$–$\varepsilon^{184}W$ correlation (Fig. 2, Table 2).

The initial $^{182}Hf/^{180}Hf$ and $\varepsilon^{182}W$ determined for bulk CAI in the present study are in good agreement with an initial $^{182}Hf/^{180}Hf$ of $(9.85 \pm 0.40) \times 10^{-5}$ and $\varepsilon^{182}W_i = -3.51 \pm 0.10$ reported by Burkhardt et al. (2012) for an Hf–W isochron for mineral separates of coarse-grained CAI. The initial $\varepsilon^{182}W$ reported by Burkhardt et al. (2012) was not only based on the $\varepsilon^{182}W_i$ *vs.* $\varepsilon^{183}W$ correlation defined by several bulk CAI, but also on the $\varepsilon^{182}W_i$ obtained from an internal isochron corrected for nucleosynthetic W isotope variability using the mean $\varepsilon^{183}W$ of all CAI used in the regression and using the theoretical model of Arlandini et al. (1999). Note that because these corrections were small for most of the CAI investi-

gated by Burkhardt et al. (2012), using the Arlandini et al. slope of ~1.686 instead of the ~1.41 slope determined here for bulk CAI does not result in resolvable differences. MacPherson et al. (2012) observed that re-melted, coarse-grained CAI have a range in initial $^{26}Al/^{27}Al$ ratios corresponding to a time interval of ~0.2 Ma. In contrast, primitive, unmelted CAI show no differences in their initial $^{26}Al/^{27}Al$, which also is indistinguishable from that obtained from a bulk CAI Al–Mg isochron. The Al–Mg data, therefore, provide evidence that some CAI have been reprocessed for at least ~0.2 Ma after initial CAI formation. Although such a small time difference cannot be resolved using Hf–W chronometry, the Al–Mg data nevertheless show that the initial $^{182}Hf/^{180}Hf$ and $\varepsilon^{182}W$ at the time of primary CAI formation and, hence, at 'time zero' of solar system history is best defined by a bulk CAI isochron.

6. Comparison to ^{26}Al–^{26}Mg ages and evidence for ^{26}Al homogeneity

The use of short-lived chronometers like ^{26}Al–^{26}Mg and ^{182}Hf–^{182}W relies on the assumption that the parent nuclides were homogeneously distributed in the early solar system. Especially for the ^{26}Al–^{26}Mg system the validity of this assumption is debated, however. For instance, the discovery of refractory inclusions with low initial ^{26}Al abundances (*e.g.*, Lee et al., 1979) as well as the presence of ^{26}Al-rich and ^{26}Al-poor refractory grains in primitive meteorites (*e.g.*, Ireland, 1990; Krot et al., 2009; Liu et al., 2012; Makide et al., 2011) bear testimony to a heterogeneous distribution of ^{26}Al at the beginning of solar system history. This raises the question whether this early small-scale heterogeneity of ^{26}Al extends to the bulk meteorite scale, in which case variable $^{26}Al/^{27}Al$ in meteorites and meteorite components may have no chronological meaning (*e.g.*, Clayton et al., 1977; Gounelle et al., 2001; Larsen et al., 2011; Lee, 1978). The level of ^{26}Al heterogeneity at the bulk meteorite scale can be tested through inter-calibration of different short-lived and long-lived chronometers between CAI and other well-dated samples (*e.g.*, Amelin et al., 2002; Bouvier et al., 2011b; Nyquist et al., 2009). Angrites are the ideal samples for such an inter-calibration, because the rapid cooling of these samples ensures that differences in closure temperatures between the various chronometers do not result in resolvable age differences (Kleine et al., 2012; Lugmair and Galer, 1992; Markowski et al., 2007; Nyquist et al., 2009; Spivak-Birndorf et al., 2009). Thus, the age intervals given by the different chronometers between CAI formation and crystallization of angrites can be directly compared.

A recent Hf–W study of angrites reported indistinguishable initial $^{182}Hf/^{180}Hf$ of $(7.15 \pm 0.17) \times 10^{-5}$ and $(6.87 \pm 0.15) \times 10^{-5}$ for the quenched angrites D'Orbigny and Sahara 99555 (Kleine et al., 2012). Using the newly determined solar system initial $^{182}Hf/^{180}Hf$ of $(1.018 \pm 0.043) \times 10^{-4}$, formation intervals relative to CAI formation, Δt_{CAI}, of 4.5 ± 0.6 Ma and 5.1 ± 0.6 Ma are inferred for these two angrites (Fig. 5). A combined isochron for D'Orbigny and Sahara 99555 yields an initial $^{182}Hf/^{180}Hf$ of $(6.99 \pm 0.11) \times 10^{-5}$, corresponding to $\Delta t_{CAI} = 4.8 \pm 0.6$ Ma (2σ). The Al–Mg isochrons determined for D'Orbigny and Sahara 99555 also yield indistinguishable initial $^{26}Al/^{27}Al$ for these two angrites, corresponding to formation intervals relative to CAI [$^{26}Al/^{27}Al = (5.23 \pm 0.13) \times 10^{-5}$ (Jacobsen et al., 2008)] of 4.7 ± 0.2 Ma (Spivak-Birndorf et al., 2009) or 5.0 ± 0.1 Ma (Schiller et al., 2010) [using a ^{26}Al half-life of 0.708 ± 0.017 Myr (Nishiizumi, 2004)]. Both Al–Mg ages for D'Orbigny and Sahara 99555 are in excellent agreement with $\Delta t_{CAI} = 4.8 \pm 0.6$ Ma as obtained from Hf–W chronometry (Fig. 5). Note that the nominal Hf–W age for D'Orbigny and Sahara 99555 is ~0.6 Ma younger than that calculated by Kleine et al. (2012) using the previously inferred solar system initial $^{182}Hf/^{180}Hf$ of $(9.72 \pm 0.44) \times 10^{-5}$ (Burkhardt et al., 2008), bringing the Hf–W and Al–Mg ages of these angrites in better agreement than previously recognized.

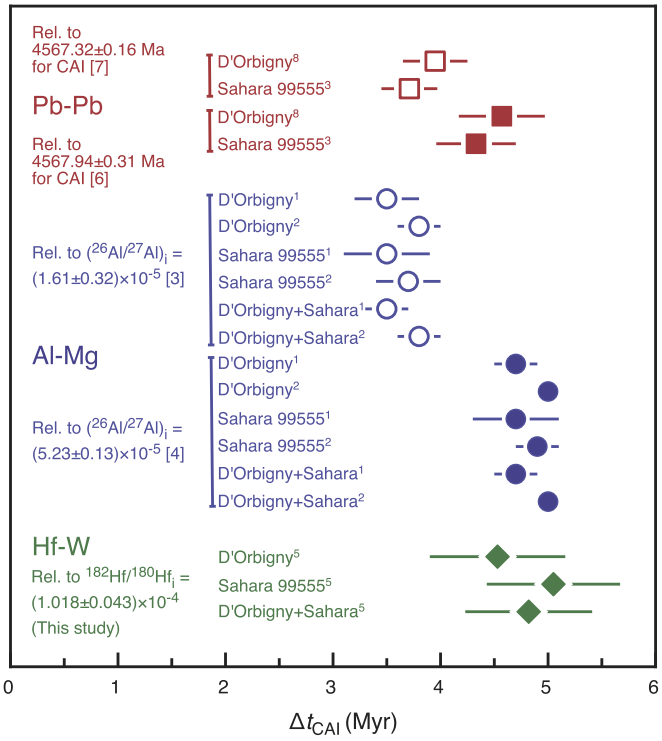

Fig. 5. Comparison of Pb–Pb, Al–Mg, and Hf–W ages relative to CAI formation for the angrites D'Orbigny and Sahara 99555. Open symbols show Al–Mg ages calculated relative to the proposed initial $^{26}Al/^{27}Al$ of $(1.61 \pm 0.32) \times 10^{-5}$ for the angrite precursor at the time of CAI formation (Larsen et al., 2011). Closed symbols show Al–Mg ages calculated relative to the canonical initial $^{26}Al/^{27}Al$ of $(5.23 \pm 0.13) \times 10^{-5}$ (Jacobsen et al., 2008). Hf–W ages were calculated relative to an initial $^{182}Hf/^{180}Hf = (1.018 \pm 0.043) \times 10^{-4}$ determined in this study. Pb–Pb formation intervals for angrites were either calculated relative to the Pb–Pb age of CAI NWA 6991 B4 (filled symbols) or to the average age obtained for three Efremovka CAI (open symbols). Data sources: (1) Spivak-Birndorf et al. (2009), (2) Schiller et al. (2010), (3) Larsen et al. (2011), (4) Jacobsen et al. (2008), (5) Kleine et al. (2012), (6) Bouvier et al. (2011a), (7) Connelly et al. (2012), and (8) Brennecka and Wadhwa (2012). Note that only Pb–Pb ages were used which were calculated using measured U isotope compositions.

On the basis of small ^{26}Mg variations in bulk meteorites unrelated to ^{26}Al-decay, which appear to be correlated with nucleosynthetic ^{54}Cr anomalies, Larsen et al. (2011) argued that ^{26}Al was heterogeneously distributed at the bulk meteorite scale. These authors inferred an initial $^{26}Al/^{27}Al$ of the angrite parent body of $(1.61 \pm 0.32) \times 10^{-5}$ at the time of CAI formation. Relative to this initial $^{26}Al/^{27}Al$ the Al–Mg age for D'Orbigny and Sahara 99555 would be 3.5 ± 0.3 Ma (using the initial $^{26}Al/^{27}Al$ obtained by Spivak-Birndorf et al., 2009) or 3.8 ± 0.2 Ma (using the initial $^{26}Al/^{27}Al$ obtained by Schiller et al., 2010), difficult to reconcile with $\Delta t_{CAI} = 4.8 \pm 0.6$ Ma as determined by Hf–W chronometry in the present study (Fig. 5). Thus our new Hf–W data do not support the heterogeneous distribution of ^{26}Al at the bulk meteorite scale as inferred by Larsen et al. (2011), but are consistent with canonical initial $^{26}Al/^{27}Al$ of the precursor material of the angrite parent body at the time of CAI formation.

Matters become more complicated when the Hf–W and Al–Mg formation intervals are compared to those obtained from Pb–Pb chronometry. Given the evidence for U isotope variability among meteorites and especially CAI, precise Pb–Pb ages can only be obtained in concert with U isotope measurements on the same samples (Brennecka et al., 2010). Available U-corrected Pb–Pb ages for CAI are 4567.18 ± 0.50 Ma (Amelin et al., 2010), 4567.32 ± 0.16 Ma (mean for three fine- and coarse-grained CAI;

Connelly et al., 2012), and 4567.94 ± 0.31 Ma (Bouvier et al., 2011a). The reason for the slight disparity among these ages is unclear at present, making the absolute age of CAI and, hence, Pb–Pb formation intervals relative to CAI, uncertain by ~0.6 Ma (*i.e.*, the difference between current U-corrected Pb–Pb ages). Relative to an age of 4567.32 ± 0.16 Ma for CAI, the Pb–Pb formation intervals for D'Orbigny and Sahara 99555—using their U-corrected Pb–Pb ages (Brennecka and Wadhwa, 2012; Larsen et al., 2011)—are 3.95 ± 0.30 Ma and 3.71 ± 0.26 Ma, inconsistent with $\Delta t_{CAI} = 4.8 \pm 0.6$ Ma as determined by Hf–W chronometry. Relative to an age of 4567.94 ± 0.31 Ma for CAI, the formation intervals of D'Orbigny and Sahara 99555 become 4.57 ± 0.40 Ma and 4.33 ± 0.37 Ma, however, consistent with the Hf–W and Al–Mg ages for these two angrites (Fig. 5). Note that Larsen et al. (2011) argued that the Pb–Pb systematics support their model for a heterogeneous distribution of ^{26}Al, because the Pb–Pb formation interval between Sahara 99555 and CAI is shorter than that obtained from Al–Mg chronometry assuming a canonical ^{26}Al/^{27}Al of the angrite precursors at the time of CAI formation. As shown here, this conclusion is dependent on the choice of the Pb–Pb age for CAI, however (Fig. 5). It thus appears that Pb–Pb isotope systematics currently cannot unequivocally distinguish between a homogeneous and heterogeneous distribution of ^{26}Al in the solar protoplanetary disk. In contrast, the good agreement between the Al–Mg and Hf–W formation intervals between angrites and CAI is inconsistent with a grossly heterogeneous distribution of ^{26}Al, at least in the nebular regions were CAI and angrites formed.

Our results imply that the correlation of ^{26}Mg and ^{54}Cr observed for bulk meteorites and CAI by Larsen et al. (2011) more likely reflects nucleosynthetic Mg (and Cr) isotope variations rather than ^{26}Al heterogeneity. This is consistent with the evidence for nucleosynthetic Mg isotope anomalies in CAI characterized by canonical ^{26}Al/^{27}Al (Wasserburg et al., 2012). Thus, it appears that variations in initial ^{26}Al/^{27}Al ratios of bulk meteorites and most meteorite components have chronological significance (*e.g.*, Bouvier et al., 2011b; Mishra and Chaussidon, 2014; Villeneuve et al., 2009; Wasserburg et al., 2012), whereas small variations in ^{26}Mg/^{24}Mg among bulk meteorites may have not.

Acknowledgements

We thank two anonymous reviewers for their comments that helped to improve the manuscript, and also thank Chris Coath for additional constructive comments. Tim Elliott is gratefully acknowledged for his editorial efforts and helpful comments. TSK thanks G. Budde, D. Cook and P. Sprung for fruitful discussions. U. Heitmann, T. Grund, I. Ivanov-Bucher, and M. Matthes are gratefully acknowledged for their technical support. This study was supported by a Förderungsprofessur of the Swiss National Science Foundation to T. Kleine (Grant no. PP00P2_123470) and by the Deutsche Forschungsgemeinschaft (KL 1857/3) within the Research Priority Programme 1385.

Appendix A. Supplementary material

Supplementary material related to this article can be found online at http://dx.doi.org/10.1016/j.epsl.2014.07.003.

References

Amelin, Y., Kaltenbach, A., Iizuka, T., Stirling, C.H., Ireland, T.R., Petaev, M., Jacobsen, S.B., 2010. U–Pb chronology of the Solar System's oldest solids with variable ^{238}U/^{235}U. Earth Planet. Sci. Lett. 300, 343–350.

Amelin, Y., Krot, A.N., Hutcheon, I.D., Ulyanov, A.A., 2002. Lead isotopic ages of chondrules and calcium–aluminum-rich inclusions. Science 297, 1678–1683.

Arlandini, C., Kappeler, F., Wisshak, K., Gallino, R., Lugaro, M., Busso, M., Straniero, O., 1999. Neutron capture in low-mass asymptotic giant branch stars: cross sections and abundance signatures. Astrophys. J. 525, 886–900.

Ávila, J.N., Lugaro, M., Ireland, T.R., Gyngard, F., Zinner, E., Cristallo, S., Holden, P., Buntain, J., Amari, S., Karakas, A., 2012. Tungsten isotopic compositions in stardust SiC grains from the Murchison meteorite: constraints on the s-process in the Hf–Ta–W–Re–Os region. Astrophys. J. 744, 49.

Bouvier, A., Brennecka, G.A., Wadhwa, M., 2011a. Absolute chronology of the first solids in the solar system. Workshop on formation of the first solids in the Solar System (#9054), Hawaii.

Bouvier, A., Spivak-Birndorf, L.J., Brennecka, G.A., Wadhwa, M., 2011b. New constraints on early Solar System chronology from Al–Mg and U–Pb isotope systematics in the unique basaltic achondrite Northwest Africa 2976. Geochim. Cosmochim. Acta 75, 5310–5323.

Bouvier, A., Wadhwa, M., 2010. The age of the Solar System redefined by the oldest Pb–Pb age of a meteoritic inclusion. Nat. Geosci. 3, 637–641.

Boynton, W.V., 1975. Fractionation in the solar nebula: condensation of yttrium and the rare earth elements. Geochim. Cosmochim. Acta 39, 569–584.

Brennecka, G.A., Wadhwa, M., 2012. Uranium isotope compositions of the basaltic angrite meteorites and the chronological implications for the early Solar System. Proc. Natl. Acad. Sci. USA 109, 9299–9303.

Brennecka, G.A., Weyer, S., Wadhwa, M., Janney, P.E., Zipfel, J., Anbar, A.D., 2010. ^{238}U/^{235}U variations in meteorites: extant ^{247}Cm and implications for Pb–Pb dating. Science 327, 449.

Burkhardt, C., Kleine, T., Bourdon, B., Palme, H., Zipfel, J., Friedrich, J.M., Ebel, D.S., 2008. Hf–W mineral isochron for Ca, Al-rich inclusions: age of the solar system and the timing of core formation in planetesimals. Geochim. Cosmochim. Acta 72, 6177–6197.

Burkhardt, C., Kleine, T., Dauphas, N., Wieler, R., 2012. Nucleosynthetic tungsten isotope anomalies in acid leachates of the Murchison chondrite: implications for hafnium-tungsten chronometry. Astrophys. J. Lett. 753, L6.

Burkhardt, C., Schönbächler, M., 2013. Nucleosynthetic tungsten isotope anomalies in acid leachates of the Orgueil, Murchison, and Allende carbonaceous chondrites. In: Lunar and Planetary Science Conference (#1912). Houston, TX.

Clayton, D.D., Dwek, E., Woosley, S.E., 1977. Isotopic anomalies and proton irradiation in the early solar system. Astrophys. J. 214, 300–315.

Connelly, J.N., Bizzarro, M., Krot, A.N., Nordlund, Å., Wielandt, D., Ivanova, M.A., 2012. The absolute chronology and thermal processing of solids in the solar protoplanetary disk. Science 338, 651–655.

Davis, A.M., Grossman, L., 1979. Condensation and fractionation of rare earths in the solar nebula. Geochim. Cosmochim. Acta 43, 1611–1632.

Gounelle, M., Russell, S.S., 2005. On early Solar System chronology: implications of an heterogeneous spatial distribution of ^{26}Al and ^{53}Mn. Geochim. Cosmochim. Acta 69, 3129–3144.

Gounelle, M., Shu, F.H., Shang, H., Glassgold, A.E., Rehm, K.E., Lee, T., 2001. Extinct radioactivities and protosolar cosmic rays: self-shielding and light elements. Astrophys. J. 548, 1051.

Gray, C.M., Papanastassiou, D.A., Wasserburg, G.J., 1973. Identification of early condensates from the Solar Nebula. Icarus 20, 213–239.

Grossman, L., Ganapathy, R., 1976. Trace elements in the Allende meteorite—II. Fine-grained, Ca-rich inclusions. Geochim. Cosmochim. Acta 40, 967–977.

Humayun, M., Simon, S.B., Grossman, L., 2007. Tungsten and hafnium distribution in calcium–aluminum inclusions (CAIs) from Allende and Efremovka. Geochim. Cosmochim. Acta 71, 4609–4627.

Ireland, T.R., 1990. Presolar isotopic and chemical signatures in hibonite-bearing refractory inclusions from the Murchison carbonaceous chondrite. Geochim. Cosmochim. Acta 54, 3219–3237.

Jacobsen, B., Yin, Q.Z., Moynier, F., Amelin, Y., Krot, A.N., Nagashima, K., Hutcheon, I.D., Palme, H., 2008. Al-26–Mg-26 and Pb-207–Pb-206 systematics of Allende CAIs: canonical solar initial Al-26/Al-27 ratio reinstated. Earth Planet. Sci. Lett. 272, 353–364.

Kleine, T., Hans, U., Irving, A.J., Bourdon, B., 2012. Chronology of the angrite parent body and implications for core formation in protoplanets. Geochim. Cosmochim. Acta 84, 186–203.

Kleine, T., Mezger, K., Munker, C., Palme, H., Bischoff, A., 2004. Hf-182–W-182 isotope systematics of chondrites, eucrites, and martian meteorites: chronology of core formation and early mantle differentiation in Vesta and Mars. Geochim. Cosmochim. Acta 68, 2935–2946.

Kleine, T., Mezger, K., Palme, H., Scherer, E., Munker, C., 2005. Early core formation in asteroids and late accretion of chondrite parent bodies: evidence from Hf-182–W-182 in CAIs, metal-rich chondrites, and iron meteorites. Geochim. Cosmochim. Acta 69, 5805–5818.

Kleine, T., Munker, C., Mezger, K., Palme, H., 2002. Rapid accretion and early core formation on asteroids and the terrestrial planets from Hf–W chronometry. Nature 418, 952–955.

Kleine, T., Touboul, M., Bourdon, B., Nimmo, F., Mezger, K., Palme, H., Jacobsen, S.B., Yin, Q.Z., Halliday, A.N., 2009. Hf–W chronology of the accretion and early evolution of asteroids and terrestrial planets. Geochim. Cosmochim. Acta 73, 5150–5188.

Kornacki, A.S., Wood, J.A., 1985. Mineral chemistry and origin of spinel-rich inclusions in the Allende CV3 chondrite. Geochim. Cosmochim. Acta 49, 1219–1237.

Krot, A.N., Amelin, Y., Bland, P., Ciesla, F.J., Connelly, J., Davis, A.M., Huss, G.R., Hutcheon, I.D., Makide, K., Nagashima, K., Nyquist, L.E., Russell, S.S., Scott, E.R.D.,

Thrane, K., Yurimoto, H., Yin, Q.Z., 2009. Origin and chronology of chondritic components: a review. Geochim. Cosmochim. Acta 73, 4963–4997.

Krot, A.N., Scott, E.R.D., Zolensky, M.E., 1995. Mineralogical and chemical modification of components in CV3 chondrites: nebular or asteroidal processing? Meteoritics 30, 748–775.

Kruijer, T.S., Fischer-Gödde, M., Kleine, T., Sprung, P., Leya, I., Wieler, R., 2013. Neutron capture on Pt isotopes in iron meteorites and the Hf–W chronology of core formation in planetesimals. Earth Planet. Sci. Lett. 361, 162–172.

Kruijer, T.S., Sprung, P., Kleine, T., Leya, I., Burkhardt, C., Wieler, R., 2012. Hf–W chronometry of core formation in planetesimals inferred from weakly irradiated iron meteorites. Geochim. Cosmochim. Acta 99, 287–304.

Larsen, K.K., Trinquier, A., Paton, C., Schiller, M., Wielandt, D., Ivanova, M.A., Connelly, J.N., Nordlund, Å., Krot, A.N., Bizzarro, M., 2011. Evidence for magnesium isotope heterogeneity in the solar protoplanetary disk. Astrophys. J. Lett. 735, L37.

Lee, T., 1978. A local proton irradiation model for isotopic anomalies in the solar system. Astrophys. J. 224, 217–226.

Lee, T., Papanastassiou, D.A., Wasserburg, G.J., 1976. Demonstration of Mg-26 excess in Allende and evidence for Al-26. Geophys. Res. Lett. 3, 109–112.

Lee, T., Papanastassiou, D.A., Wasserburg, G.J., 1977. Aluminum-26 in the early solar system: fossil or fuel? Astrophys. J. Lett. 211, L107–L110.

Lee, T., Russell, W.A., Wasserburg, G.J., 1979. Calcium isotopic anomalies and the lack of aluminium-26 in an unusual Allende inclusion. Astrophys. J. 228, L93–L98.

Leya, I., 2011. Cosmogenic effects on ^{7}Li/^{6}Li, ^{10}B/^{11}B, and ^{182}W/^{184}W in CAIs from carbonaceous chondrites. Geochim. Cosmochim. Acta 75, 1507–1518.

Leya, I., Schonbachler, M., Krahenbuhl, U., Halliday, A.N., 2009. New titanium isotope data for Allende and Efremovka CAIs. Astrophys. J. 702, 1118–1126.

Leya, I., Wieler, R., Halliday, A.N., 2003. The influence of cosmic-ray production on extinct nuclide systems. Geochim. Cosmochim. Acta 67, 529–541.

Liu, M.-C., Chaussidon, M., Göpel, C., Lee, T., 2012. A heterogeneous solar nebula as sampled by CM hibonite grains. Earth Planet. Sci. Lett. 327–328, 75–83.

Lodders, K., 2003. Solar system abundances and condensation temperatures of the elements. Astrophys. J. 591, 1220–1247.

Lugmair, G.W., Galer, S.J.G., 1992. Age and isotopic relationships among the angrites Lewis Cliff 86010 and Angra dos Reis. Geochim. Cosmochim. Acta 56, 1673–1694.

MacPherson, G.J., Davis, A.M., Zinner, E.K., 1995. The distribution of Al-26 in the Early Solar-System – a reappraisal. Meteoritics 30, 365–386.

MacPherson, G.J., Kita, N.T., Ushikubo, T., Bullock, E.S., Davis, A.M., 2012. Well-resolved variations in the formation ages for Ca–Al-rich inclusions in the early Solar System. Earth Planet. Sci. Lett. 331–332, 43–54.

Makide, K., Nagashima, K., Krot, A.N., Huss, G.R., Ciesla, F.J., Hellebrand, E., Gaidos, E., Yang, L., 2011. Heterogeneous distribution of ^{26}Al at the birth of the Solar System. Astrophys. J. Lett. 733, L31.

Markowski, A., Quitte, G., Kleine, T., Halliday, A.N., Bizzarro, M., Irving, A.J., 2007. Hafnium–tungsten chronometry of angrites and the earliest evolution of planetary objects. Earth Planet. Sci. Lett. 262, 214–229.

Mishra, R.K., Chaussidon, M., 2014. Timing and extent of Mg and Al isotopic homogenization in the early inner Solar System. Earth Planet. Sci. Lett. 390, 318–326.

Niemeyer, S., Lugmair, G.W., 1981. Ubiquitous isotopic anomalies in Ti from normal Allende inclusions. Earth Planet. Sci. Lett. 53, 211–225.

Nishiizumi, K., 2004. Preparation of ^{26}Al AMS standards. Nucl. Instrum. Methods Phys. Res., Sect. B, Beam Interact. Mater. Atoms 223–224, 388–392.

Nyquist, L.E., Kleine, T., Shih, C.Y., Reese, Y.D., 2009. The distribution of short-lived radioisotopes in the early solar system and the chronology of asteroid accretion, differentiation, and secondary mineralization. Geochim. Cosmochim. Acta 73, 5115–5136.

Podosek, F.A., Zinner, E.K., MacPherson, G.J., Lundberg, L.L., Brannon, J.C., Fahey, A.J., 1991. Correlated study of initial ^{87}Sr/^{86}Sr and Al–Mg isotopic systematics and petrologic properties in a suite of refractory inclusions from the Allende meteorite. Geochim. Cosmochim. Acta 55, 1083–1110.

Qin, L.P., Dauphas, N., Wadhwa, M., Markowski, A., Gallino, R., Janney, P.E., Bouman, C., 2008. Tungsten nuclear anomalies in planetesimal cores. Astrophys. J. 674, 1234–1241.

Scherer, P., Schultz, L., 2000. Noble gas record, collisional history, and pairing of CV, CO, CK, and other carbonaceous chondrites. Meteorit. Planet. Sci. 35, 145–153.

Schiller, M., Baker, J.A., Bizzarro, M., 2010. Al-26–Mg-26 dating of asteroidal magmatism in the young Solar System. Geochim. Cosmochim. Acta 74, 4844–4864.

Shirai, N., Humayun, M., 2011. Mass independent bias in W isotopes in MC-ICP-MS instruments. J. Anal. At. Spectrom. 26, 1414–1420.

Spivak-Birndorf, L., Wadhwa, M., Janney, P., 2009. ^{26}Al–^{26}Mg systematics in D'Orbigny and Sahara 99555 angrites: implications for high-resolution chronology using extinct chronometers. Geochim. Cosmochim. Acta 73, 5202–5211.

Villeneuve, J., Chaussidon, M., Libourel, G., 2009. Homogeneous distribution of ^{26}Al in the Solar System from the Mg isotopic composition of chondrules. Science 325, 985–988.

Wasserburg, G.J., Wimpenny, J., Yin, Q.-Z., 2012. Mg isotopic heterogeneity, Al–Mg isochrons, and canonical ^{26}Al/^{27}Al in the early solar system. Meteorit. Planet. Sci. 47, 1980–1997.

Willbold, M., Elliott, T., Moorbath, S., 2011. The tungsten isotopic composition of the Earth's mantle before the terminal bombardment. Nature 477, 195–199.

Yokoyama, T., Alexander, C.M.O.D., Walker, R.J., 2011. Assessment of nebular versus parent body processes on presolar components present in chondrites: evidence from osmium isotopes. Earth Planet. Sci. Lett. 305, 115–123.